THE DYNAMIC RESPONSE OF A PLANETARY GEAR TRAIN IN THE PRESENCE OF A SPALLING FAULT

Keming Zhang, Yimin Shao , Diego Galar*
State Key Laboratory of Mechanical Transmission
Shazheng Street 174
Shapingba District
Chongqing, 400044, CHINA
ymshao@cqu.edu.cn
*Division of Operation and Maintenance Engineering
Lulea University of Technology
Lulea 97187, SWEDEN

Abstract: Planetary gear trains (PGTs) are widely used in industrial applications. Failure often occurs under working conditions. Tooth surface spalling is one of the most common defects in a PGT system; it seriously affects the reliability and safety of the mechanical transmission system and may even cause serious incidents. However, research into the faults of planetary gear trains is insufficient, especially with respect to the response characteristics of a PGT in the presence of a spalling defect. The paper designs spalling cases with different localized distributions to demonstrate their influence on the dynamic performance of the planetary gear set. The research provides a theoretical basis for health diagnosis and early fault detection for a PGT system.

Key words: Planetary gear train; spalling defect; dynamic performance;

Introduction:

Planetary gear trains (PGTs) are widely used in industrial applications because they can operate in many different conditions. Tooth spalling is one of the most common failure modes [1]. When a spalling fault appears on a gear tooth, the mesh stiffness will reduce and the dynamic vibration properties of the system will change, leading to the shutdown of the whole system. Establishing a dynamic model of a planetary gear train with a spalling defect and studying the vibration response characteristics of the system would help to monitor the health of a PGT system and detect incipient failures.

Many researchers have studied the vibration properties of PGT systems. Kim [2] established a dynamic model with time-varying pressure angles and contact ratios to investigate their effects on the dynamic behavior of a planetary gear. Kahraman [3-4] used two- and three-dimensional models to examine the dynamic response of both time-invariant and time-varying representations. Kahraman and Vijayakar [5] investigated the effect of internal gear flexibility on the quasi-static behavior of a planetary gear set by using a finite element/semi-analytical nonlinear contact mechanical formulation, while Inalpolat and Kahraman [6,7] studied the modulation sidebands of planetary gear sets. Using a finite element/contact mechanics model, Parker [8] investigated the dynamic response of a planetary gear system; the calculated response showed classical resonances when the

harmonic of the mesh frequency coincided with the natural frequency. Sun and Hu [9] studied the nonlinear dynamics of a planetary gear system with multiple clearances, such as backlashes.

Most of the existing models focus on the system under healthy conditions. Studies of faulty planetary gear trains are insufficient, especially with respect to the response characteristics of a PGT in the presence of a localized spalling defect. To overcome this insufficiency, this study establishes a dynamic model of planetary gear sets with spalling defects. It calculates the time-varying mesh stiffness under spalling conditions, solves the responses of the defect system in the presence of a localized sun/planet/ring gear spalling defect, and analyzes the frequency distribution of response signals under these conditions. The research provides a theoretical basis for diagnosis of the PGT system and early fault detection.

Mesh Stiffness Evaluation:

Gear mesh stiffness is one of the most significant internal issues of gear dynamics. Mesh stiffness can change and when it does, the dynamic properties of the gear system will change. Therefore, accurate evaluation of gear mesh stiffness is essential for the dynamic analysis of a PGT system.

This paper uses the potential energy method proposed by Yang and Lin [10] and refined by Tian [11] and Chen et al. [12] to calculate the time varying mesh stiffness (TVMS) of gear pairs. The gear tooth is modeled as a nonuniform cantilever beam. The total energy store in the gear pair is the combination of bending energy U_b , shear energy U_s , axial compressive energy U_a, and Hertzian energy U_z which respectively correspond to bending stiffness K_b , shear stiffness K_s , axial compressive stiffness Ka, and Hertzian stiffness K_h.

Figure 1 shows a gear tooth modeled as a nonuniform cantilever beam. There is a spalling fault on the gear tooth surface. Without loss of generality, the spalling is modeled as a rectangle with dimensions $w \times l_s$ in Figure 2. The depth of the spalling defect is h_s and the width of the gear tooth is L. As shown in Figure 2 and described in more detail below, there are three stages in spalling.

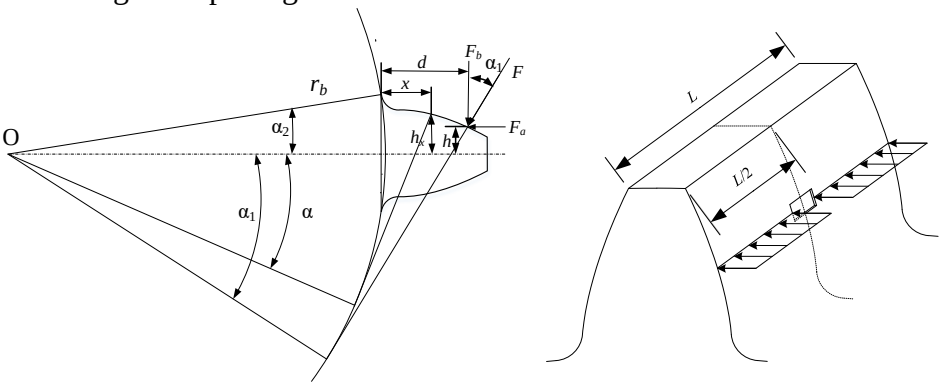

Figure 1: Gear tooth model with spalling defect

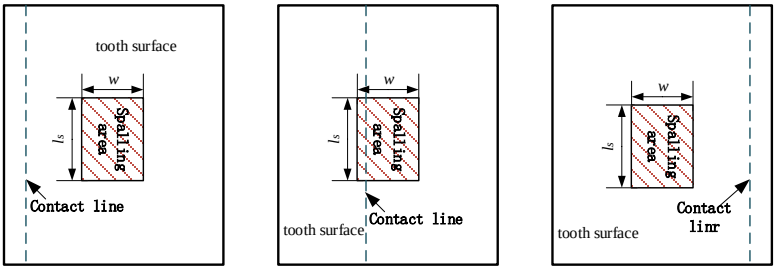

Figure 2: Three stages of spalling

Stage 1: The contact line is below the spalling area in stage 1, as shown in Figure 2(a). In this stage, the width of contact of two meshing teeth is equal to W; the bending stiffness is Kb, shear stiffness is Ks, axial compressive stiffness is Ka, and Hertzian stiffness is Kh. These can respectively be expressed as :

$$k_b = 1/\left\{\int_{-\alpha_2}^{\alpha_1} \frac{3\left[1-\cos\alpha\cos\alpha_1-(\alpha+\alpha_2)\sin\alpha\cos\alpha_1\right]^2(\alpha+\alpha_2)\cos\alpha}{2EL\left[(\alpha+\alpha_2)\cos\alpha-\sin\alpha\right]^3}d\alpha\right\} \tag{1}$$

$$k_{s1} = 1/\left\{\int_{-\alpha_2}^{\alpha_1} \frac{1.2\cos^2\alpha_1(\alpha+\alpha_2)\cos\alpha}{2GL\left[(\alpha+\alpha_2)\cos\alpha-\sin\alpha\right]}d\alpha\right\} \tag{2}$$

$$k_{a1} = 1/\left\{\int_{-\alpha_2}^{\alpha_1} \frac{\sin^2\alpha_1(\alpha+\alpha_2)\cos\alpha}{2EL\left[(\alpha+\alpha_2)\cos\alpha-\sin\alpha\right]}d\alpha\right\} \tag{3}$$

$$k_h = \frac{\pi EL}{4(1-\nu^2)} \tag{4}$$

where L is the tooth width, α_1 is the acting pressure angle of gear tooth, E denotes the modulus of elasticity, and v denotes the Poisson ratio.

Stage 2: The contact line is engaged in the spalling area in stage 2, as shown in Figure 2(b). In this stage, the spalling area does not engage with the meshing; the length of the contact line changes from L to L-l_s. Correspondingly, the Hertzian stiffness decreases, and can be expressed as:

$$k_h = \frac{\pi E(L-l_s)}{4(1-\nu^2)} \tag{5}$$

In addition, computation of the TVMS has to take into account the shape of the elementary cross-sectional area and the moment of inertia, as both of these will change. The bending stiffness, shear stiffness, and axial compression stiffness can respectively be expressed as follows:

$$k_b = 1/\left(\int_{-\alpha_2}^{\alpha_{s2}} \frac{3\left[1-\cos\alpha\cos\alpha_1-(\alpha+\alpha_2)\sin\alpha\cos\alpha_1\right]^2(\alpha+\alpha_2)\cos\alpha}{2EL\left[(\alpha+\alpha_2)\cos\alpha-\sin\alpha\right]^3}d\alpha + \int_{\alpha_{s2}}^{\alpha_1} \frac{12F^2R_b^3\left[1-\cos\alpha\cos\alpha_1-(\alpha+\alpha_2)\sin\alpha\cos\alpha_1\right]^2(\alpha+\alpha_2)\cos\alpha}{E\left\{8LR_b^3\left[(\alpha+\alpha_2)\cos\alpha-\sin\alpha\right]^3-h_s^3l_s\right\}}d\alpha\right) \tag{6}$$

$$k_s = 1/\left(\int_{-\alpha_2}^{\alpha_{s2}} \frac{1.2R_b(\cos\alpha_1)^2(\alpha+\alpha_2)\cos\alpha}{2GL\left[(\alpha+\alpha_2)\cos\alpha-\sin\alpha\right]}d\alpha + \int_{\alpha_{s2}}^{\alpha_1} \frac{1.2(\cos\alpha_1)^2(\alpha+\alpha_2)\cos\alpha}{G\left\{2LR_b\left[(\alpha+\alpha_2)\cos\alpha-\sin\alpha\right]-h_s l_s\right\}}d\alpha \right) \quad (7)$$

$$k_a = 1/\left(\int_{-\alpha_2}^{\alpha_{s2}} \frac{\sin^2\alpha_1(\alpha+\alpha_2)\cos\alpha}{2EL\left[(\alpha+\alpha_2)\cos\alpha-\sin\alpha\right]}d\alpha + \int_{\alpha_{s2}}^{\alpha_1} \frac{R_b\sin^2\alpha_1(\alpha+\alpha_2)\cos\alpha}{E\left\{2R_bL\left[(\alpha+\alpha_2)\cos\alpha-\sin\alpha\right]-h_s l_s\right\}}d\alpha \right) \quad (8)$$

where α_{s2} denotes the angle of pressure corresponding to the starting point of the spalling defect.

Stage 3: When the meshing line passes the end of the spalling area, stage 3 begins. In this stage, even though the spalling area is not engaged, the spalling will affect the elementary moment of inertia and the cross-sectional area of the gear, so the gear bending stiffness, shear stiffness, and axial compressive stiffness will change because of the spalling fault, and can respectively be expressed as:

$$\begin{aligned} k_b = & \int_{-\alpha_2}^{\alpha_{s2}} \frac{3\left[1-\cos\alpha\cos\alpha_1-(\alpha+\alpha_2)\sin\alpha\cos\alpha_1\right]^2(\alpha+\alpha_2)\cos\alpha}{2EL\left[(\alpha+\alpha_2)\cos\alpha-\sin\alpha\right]^3}d\alpha \\ & + \int_{\alpha_{s2}}^{\alpha_{s1}} \frac{12F^2R_b^3\left[1-\cos\alpha\cos\alpha_1-(\alpha+\alpha_2)\sin\alpha\cos\alpha_1\right]^2(\alpha+\alpha_2)\cos\alpha}{E\left\{8LR_b^3\left[(\alpha+\alpha_2)\cos\alpha-\sin\alpha\right]^3-h_s^3 l_s\right\}}d\alpha \\ & + \int_{\alpha_{s1}}^{\alpha_1} \frac{3F^2\left[1-\cos\alpha\cos\alpha_1-(\alpha+\alpha_2)\sin\alpha\cos\alpha_1\right]^2(\alpha+\alpha_2)\cos\alpha}{2EL\left[(\alpha+\alpha_2)\cos\alpha-\sin\alpha\right]^3}d\alpha \end{aligned} \quad (9)$$

$$\begin{aligned} k_s = 1/\Bigg(& \int_{-\alpha_2}^{\alpha_{s2}} \frac{1.2(\cos\alpha_1)^2(\alpha+\alpha_2)\cos\alpha}{2GL\left[(\alpha+\alpha_2)\cos\alpha-\sin\alpha\right]}d\alpha + \int_{\alpha_{s2}}^{\alpha_{s1}} \frac{1.2(\cos\alpha_1)^2(\alpha+\alpha_2)\cos\alpha}{G\left\{2LR_b\left[(\alpha+\alpha_2)\cos\alpha-\sin\alpha\right]-h_s l_s\right\}}d\alpha \\ & + \int_{\alpha_{s1}}^{\alpha_1} \frac{1.2F^2(\cos\alpha_1)^2(\alpha+\alpha_2)\cos\alpha}{4GL\left[(\alpha+\alpha_2)\cos\alpha-\sin\alpha\right]}d\alpha \Bigg) \end{aligned} \quad (10)$$

$$\begin{aligned} k_a = 1/\Bigg(& \int_{-\alpha_2}^{\alpha_{s2}} \frac{\sin^2\alpha_1(\alpha+\alpha_2)\cos\alpha}{2EL\left[(\alpha+\alpha_2)\cos\alpha-\sin\alpha\right]}d\alpha + \int_{\alpha_{s2}}^{\alpha_{s1}} \frac{R_b\sin^2\alpha_1(\alpha+\alpha_2)\cos\alpha}{E\left\{2R_bL\left[(\alpha+\alpha_2)\cos\alpha-\sin\alpha\right]-h_s l_s\right\}}d\alpha \\ & + \int_{\alpha_{s1}}^{\alpha_1} \frac{\sin^2\alpha_1(\alpha+\alpha_2)\cos\alpha}{2EL\left[(\alpha+\alpha_2)\cos\alpha-\sin\alpha\right]}d\alpha \Bigg) \end{aligned} \quad (11)$$

where α_{s1} denotes the angle of pressure corresponding to the terminal point of the spalling defect.

With the sun and planet gear parameters shown in Table.1, in the presence of a localized sun gear spalling defect, the dimensions of the spalling fault, w, L_s, h_s, are 5, 15, and 1.5mm, respectively, and the mesh stiffness can be calculated by Equations (1-11). The single-tooth mesh stiffness and double-tooth mesh stiffness are shown in Figure 3. The simulated results show that a spalling defect leads to a bigger reduction in mesh stiffness.

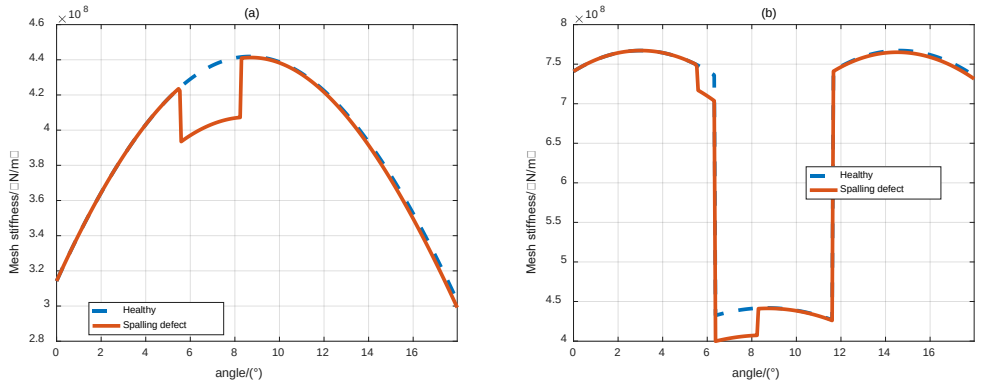

Figure 3: Mesh stiffness of sun(defect)-planet gear pair: (a) single-tooth (b) double-tooth

The internal mesh stiffness with a spalling defect is also calculated this way; because of space constraints, however, we do not discuss it here.

Dynamic Model:

The lumped-parameter model (shown in Figure 2) of the planetary gear system is used in this study to analysis the effect of a spalling fault; in this model, the mass and moment of inertia of each planet gear are identical. The planet gear rotates around the sun gear and ring gear with mesh stiffness k_{spn} and k_{rpn}, respectively, while k_{su}, k_{ru}, and k_{cu} are the support stiffness of sun, ring gear and carrier, respectively, and k_{su}, k_{ru}, and k_{cu} are the torsional stiffness of sun, ring gear and carrier, respectively. Each component contains two degrees of freedom, x_n, y_n (n=r, c, s, p), in a translational direction, and one degree of freedom, θ_m (n=r, c, s, p), in a torsional direction. The central component is a generalized displacement vector expressed as follows:

$$q = \left[x_c, y_c, \theta_c, x_r, y_r, \theta_r, x_s, y_s, \theta_s, x_1, y_1, \theta_1, \cdots, x_n, y_n, \theta_n\right]^T \tag{12}$$

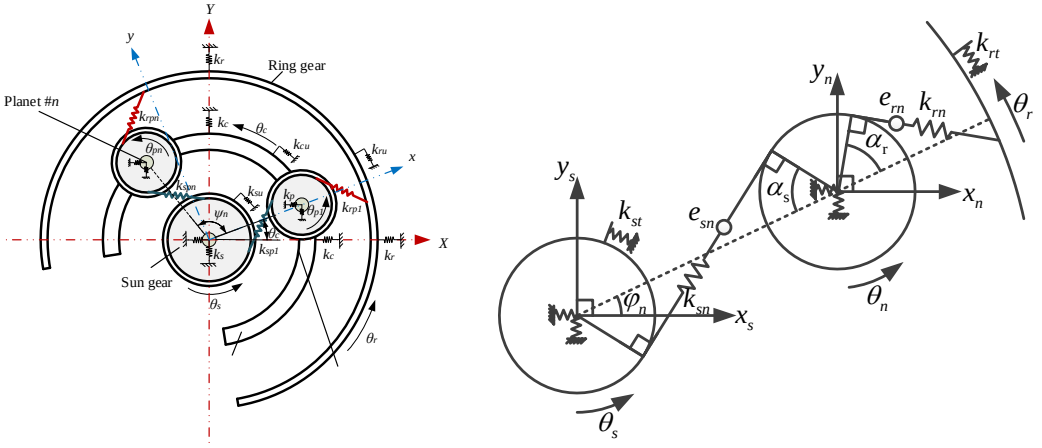

Figure 4: Dynamic model of planetary gear set

Suppose the sun gear and the carrier are the input and output component. The input torque is T_s, and the load is T_c. The ring gear is held stationary. The mass of the sun gear, carrier, ring gear, and planet gear is m_s, m_c, m_r, and m_p, respectively, and the moments of inertia

are I_s, I_c, I_r, and I_p, respectively, According to Newton's second law, the motion equation for the carrier, ring, sun gear, and planet gear can be respectively expressed as:

$$\begin{cases} m_c\ddot{x}_c + \sum k_p\delta_{cnx} + \sum c_p\dot{\delta}_{cnx} + k_c x_c + c_c\dot{x}_c = 0 \\ m_c\ddot{y}_c + \sum k_p\delta_{cny} + \sum c_p\dot{\delta}_{cny} + k_c y_c + c_c\dot{y}_c = 0 \\ \left(I_c / r_c\right)\ddot{\theta}_c + \sum k_p\delta_{cnu} + \sum c_p\dot{\delta}_{cnu} + k_{ct}\theta_c r_c + c_{ct}\dot{\theta}_c r_c = T_c / r_c \end{cases} \tag{13}$$

$$\begin{cases} m_r\ddot{x}_r - \sum k_{rn}\delta_{rn}\sin\psi_{rn} - \sum c_{rn}\dot{\delta}_{rn}\sin\psi_{rn} + k_r x_r + c_r\dot{x}_r = 0 \\ m_r\ddot{y}_r + \sum k_{rn}\delta_{rn}\cos\psi_{rn} + \sum c_{rn}\dot{\delta}_{rn}\cos\psi_{rn} + k_r y_r + c_r\dot{y}_r = 0 \\ \left(I_r / r_r\right)\ddot{\theta}_r + \sum k_{rn}\delta_{rn} + \sum c_{rn}\dot{\delta}_{rn} + k_{rt}\theta_r r_r + c_{rt}\dot{\theta}_r r_r = T_r / r_r \end{cases} \tag{14}$$

$$\begin{cases} m_s\ddot{x}_s - \sum k_{sn}\delta_{sn}\sin\psi_{sn} - \sum c_{sn}\dot{\delta}_{sn}\sin\psi_{sn} + k_s x_s + c_s\dot{x}_s = 0 \\ m_s\ddot{y}_s + \sum k_{sn}\delta_{sn}\cos\psi_{sn} + \sum c_{sn}\dot{\delta}_{sn}\cos\psi_{sn} + k_s y_s + c_s\dot{y}_s = 0 \\ \left(I_s / r_s\right)\ddot{\theta}_s + \sum k_{sn}\delta_{sn} + \sum c_{sn}\dot{\delta}_{sn} + k_{st}\theta_s r_s + c_{st}\dot{\theta}_s r_s = T_s / r_s \end{cases} \tag{15}$$

$$\begin{cases} m_n\ddot{x}_n + k_{sn}\delta_{sn}\sin\psi_{sn} + c_{sn}\dot{\delta}_{sn}\sin\psi_{sn} + k_{rn}\delta_{rn}\sin\psi_{rn} + c_{rn}\dot{\delta}_{rn}\sin\psi_{rn} - k_p\delta_{cnx} - c_p\dot{\delta}_{cnx} = 0 \\ m_n\ddot{y}_n - k_{sn}\delta_{sn}\cos\psi_{sn} - c_{sn}\dot{\delta}_{sn}\cos\psi_{sn} - k_{rn}\delta_{rn}\cos\psi_{rn} - c_{rn}\dot{\delta}_{rn}\cos\psi_{rn} - k_p\delta_{cny} - c_p\dot{\delta}_{cny} = 0 \\ \left(I_n / r_n\right)\ddot{\theta}_n + k_{sn}\delta_{sn} + c_{sn}\dot{\delta}_{sn} - k_{rn}\delta_{rn} - c_{rn}\dot{\delta}_{rn} = 0 \end{cases} \tag{16}$$

where:

$$\delta_{cnx} = x_c - x_n,\ \delta_{cny} = y_c - y_n,\ \delta_{cnu} = \left(x_n - x_c\right)\sin\psi_n + \left(y_c - y_n\right)\cos\psi_n \tag{17}$$

$$\delta_{rn} = \left(x_n - x_r\right)\sin\psi_{rn} + \left(y_r - y_n\right)\cos\psi_{rn} + \left(\theta_r - \theta_c\right)r_r - \left(\theta_n - \theta_c\right)r_n + e_{rn} \tag{18}$$

$$\delta_{sn} = \left(x_n - x_s\right)\sin\psi_{sn} + \left(y_s - y_n\right)\cos\psi_{sn} + \left(\theta_s - \theta_c\right)r_s + \left(\theta_n - \theta_c\right)r_n + e_{sn} \tag{19}$$

The dynamic analysis of a planetary gear train with a spalling fault requires a dynamic model. Depending on the location of the defect in the component, the response will be quite different; therefore, it is necessary to study the conditions of the spalling at different locations.

The spalling fault is localized on the sun gear: At setting t=0, the meshing gear pair between the sun gear and the #1 planet gear is the gear pair with the spalling defect. The tooth on the sun gear with the spalling defect has just engaged in the meshing, and the carrier is regarded as static. In this situation, the torsional displacement of the sun gear relative to the initial position can be expressed as:

$$\theta_{s\_spall} = \mathrm{mod}\left(\theta_s - \theta_c, 2\pi\right) \tag{20}$$

where mod(a,b) stands for the remainder after dividing a by b. Because there is a certain meshing phase difference between the sun gear meshing and the planet gear meshing, the torsional displacement interval between the spalling teeth of the sun gear and those of the various planetary gears is not equal to 2π/N. Consequently, the torsional displacement of the sun gear from the time when the spalling tooth begins to engage, $\theta_{s\_\mathrm{spall}\&p_i(\mathrm{in})}$, until it ceases engagement, $\theta_{s\_\mathrm{spall}\&p_i(\mathrm{out})}$, must take the meshing phase difference into consideration. This difference can be expressed as:

$$\theta_{s\_\mathrm{spall}\&p_n(\mathrm{in})} = \mathrm{floor}\left(\frac{z_s\left(n-1\right)}{N}\right) * \frac{2\pi}{z_s} + \mathrm{mod}\left(\varphi_n, \frac{2\pi}{z_s}\right) \tag{21}$$

$$\theta_{s\_\text{spall}\&p_n(\text{out})}=\text{floor}\left(\frac{z_s(n-1)}{N}\right)*\frac{2\pi}{z_s}+\text{mod}\left(\varphi_n,\frac{2\pi}{z_s}\right)+\frac{2\pi}{z_s}*e_{sp} \tag{22}$$

In Equations (21-22), floor(a) denotes a rounded to the nearest integer which is smaller than or equal to a, and e_{sp} is the contact ratio of the sun and planet gears.

If $\theta_{s\_spall\&p_n(\text{in})} \le \theta_{s\_spall} < \theta_{s\_\text{spall}\&p_n(\text{out})}$, the spalling tooth has entered into the meshing, and the meshing stiffness, k_{spn}, changes in the dynamic equation.

The spalling defect is localized on the planet gear: At setting at t=0, the meshing gear pair between the sun gear and the planet gear #1 is the gear pair with spalling. The spalling defect localized on the planet gear #1 has just entered into engaging, and the carrier is regarded as static. In this situation, the torsional displacement of the planet gear relative to the initial position can be expressed as:

$$\theta_{p_n\_\text{spall}}=\text{mod}\left(\theta_p-\theta_c,2\pi\right) \tag{23}$$

The torsional displacement of the planet gear from the time when the spalling tooth begins to engage, $\theta_{s\_\text{spall}\&p_i(\text{in})}$, to when it ends engaging, $\theta_{s\_\text{spall}\&p_i(\text{out})}$, can be expressed as:

$$\theta_{s\&p_n\_\text{spall(in)}}=0\ ,\ \theta_{s\&p_n\_\text{spall(out)}}=-\frac{2\pi}{z_p}*e_{sp} \tag{24}$$

If $\theta_{s\&p_n\_\text{spall(in)}} \le \theta_{p_n\_\text{spall}} < \theta_{s\&p_n\_\text{spall(out)}}$, the spalling tooth has entered into the meshing, and the meshing stiffness, k_{spn}, changes in the dynamic equation. However, the spalling tooth on the planet gear will also engage with the ring gear. The internal engaging of the sun & planet and the internal engaging of the planet & ring have a certain phase difference, γ_{sr}, which can be obtained following [13]. The torsional displacement of the planet gear with spalling going into and out of the inner meshing, $\theta_{r\&p_n\_\text{spall(in)}}$ and $\theta_{r\&p_n\_\text{spall(out)}}$, respectively, should take the phase difference into consideration. The difference can be expressed as:

$$\theta_{r\&p_i\_\text{spall(in)}}=-\left[\frac{2\pi*\text{ceil}\left(\frac{z_p}{2}\right)}{z_p}+\gamma_{sr}\frac{2\pi}{z_p}\right],\quad \theta_{r\&p_i\_\text{spall(out)}}=-\left[\frac{2\pi*\text{ceil}\left(\frac{z_p}{2}\right)}{z_p}+\gamma_{sr}\frac{2\pi}{z_p}+\frac{2\pi}{z_p}*e_{rp}\right] \tag{25}$$

If $\theta_{r\&p_n\_\text{spall(in)}} \le \theta_{p_n\_\text{spall}} < \theta_{r\&p_n\_\text{spall(out)}}$, the spalling tooth has entered into the meshing, and the meshing stiffness, k_{rpn}, changes in the dynamic equation.

The spalling fault is localized at the ring gear: At setting at t=0, the meshing pair between the ring gear and the #1 planet gear is the gear pair with spalling. The spalling defect on the ring gear just entered into the meshing, and the carrier is regarded as static. In this situation, the torsional displacement of the ring gear relative to the initial position can be expressed as:

$$\theta_{r\_\text{spall}}=\text{mod}\left(\theta_r-\theta_c,2\pi\right) \tag{26}$$

The torsional displacement of the sun gear with a spalling tooth from the beginning of engagement, $\theta_{r\_\text{spall}\&p_i(\text{in})}$, to the ending of engagement, $\theta_{r\_\text{spall}\&p_i(\text{out})}$, can be expressed as:

$$\theta_{r\_\text{spall}\&p_n(\text{in})} = -\left[\text{floor}\left(\frac{z_r(n-1)}{N}\right)*\frac{2\pi}{z_r} + \text{mod}\left(\varphi_n, \frac{2\pi}{z_r}\right)\right] \tag{27}$$

$$\theta_{r\_\text{spall}\&p_n(\text{out})} = -\left[\text{floor}\left(\frac{z_r(n-1)}{N}\right)*\frac{2\pi}{z_r} + \text{mod}\left(\varphi_n, \frac{2\pi}{z_r}\right) + \frac{2\pi}{z_r}*e_{rp}\right] \tag{28}$$

If $\theta_{r\_\text{spall}\&p_i(\text{in})} \le \theta_{r\_spall} < \theta_{r\_\text{spall}\&p_i(\text{out})}$, the spalling tooth has entered into the meshing, and the meshing stiffness, k_{rpn}, changes in the dynamic equation.

Numerical Simulation:

The position of the fault has a significant effect on the PGT system. In order to investigate the effect of the spalling fault and the location of the defect on the vibration properties of the system, we propose the following. A tooth surface spalling defect whose dimensions w, L_s, and h_s are 5, 15, and 1.5mm, respectively, is seeded into the sun gear, planet gear, and ring gear. The sun gear is the input component; a constant torque of 600Nm is applied to the sun gear, and its shaft speed is set at 1200rpm. The vibration properties of the PGT system with the parameters given in Table 1 are simulated.

Table 1 Parameters of the planetary gear train

	Sun	Ring	Planet	Carrier
The number of teeth	31	73	21	
Modulus (mm)	4	4	4	
pressure angle (°)	20	20	20	
mass(kg)	4.45	7.28	0.79	13.70
Moment of inertia(kg · m^2)	4.77×10^{-2}	3.72×10^{-1}	7.07×10^{-4}	2.96×10^{-1}
Support stiffness (N/m)	2×10^9	2×10^9	2×10^9	2×10^9
Torsional stiffness(Nm/rad)	0	2×10^9	0	0
Tooth width(mm)	30	30	30	

If a spalling defect is localized on the sun gear, when the spalling defect area is engaged, an impulsive vibration can be generated. Every 31 meshing cycles (the sun gear has 31 cycles), the tooth with the spalling defect will mesh with the same planet gear one time; during this period, it will also engage with the other three planet gears one time.

The torsional acceleration responses of the sun gear under two conditions (healthy and with a spalling fault) are displayed in Figure 6. The figure clearly shows impulsive vibrations resulting from the presence of the spalling tooth. When the sun gear's spalling tooth meshes

with the tooth of the planet gear, an impulsive vibration is produced. The duration of all signals given in this figure is 3*31 meshing periods *T*, corresponding to three revolutions of the sun gear (the carrier is considered static). Compared to the healthy condition, we see 12 spikes in the signal; these correspond to the spalling defect pair meshing with the planets four times in one revolution of the sun gear (there are four planets). The fault symptom is obvious.

Besides the responses in the time domain, the dynamic features in the frequency domain also exhibit the effects of a defect. According to [14], when the harmonic component of the meshing frequency is l=3, the motion of the torsional direction is excited. Figure 6 shows the frequency spectrum of the simulated acceleration signal corresponding to Figure 5. In this figure, sizable amplitudes appear at the triple harmonics of mesh frequency in two cases. The healthy case is characterized by the dominance of the mesh frequency and its harmonics, while in the case of a spalling fault on the sun gear tooth, a large number of sidebands appear around the meshing frequency and its harmonics. The frequency interval between sidebands is the characteristic frequency of the PGT with a spalling fault on the sun gear, or $N*(f_s-f_c)$ = 56.15Hz. In this case, we observe the defect signal's modulation of the amplitude of the mesh signal; this occurs once per revolution of a sun gear relative to the carrier.

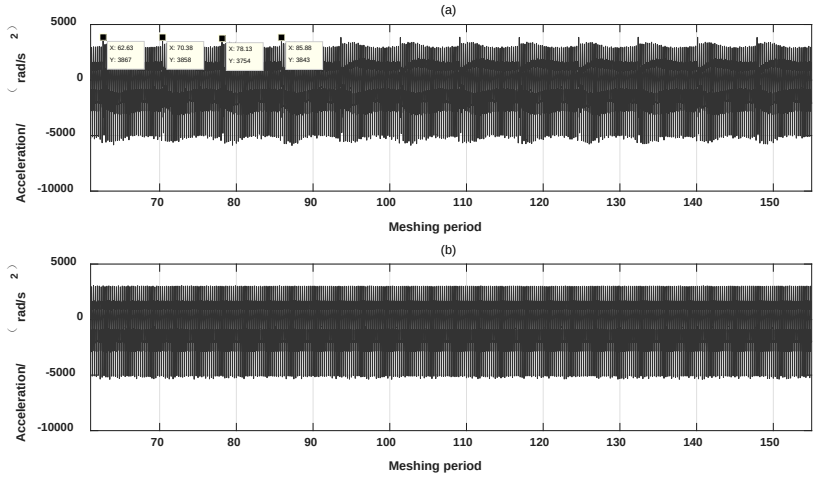

Figure 5. The dynamic response of the sun gear in torsional direction: (a) spalling fault localized on the sun gear (b) healthy planetary system

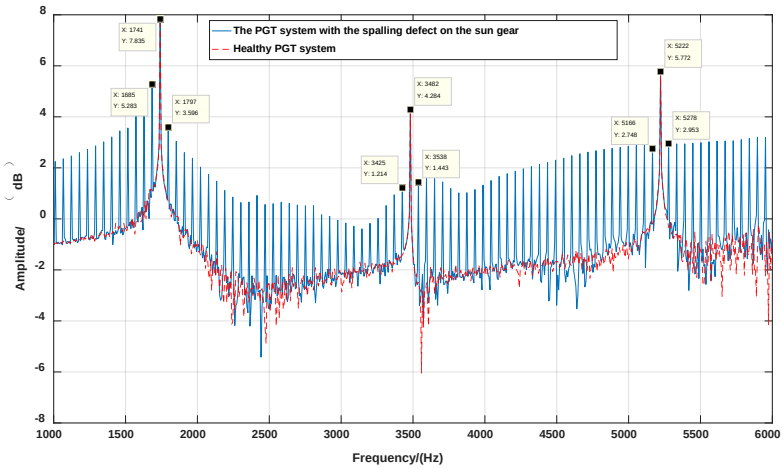

Figure 6. The frequency spectrum of the dynamic response of the sun gear in torsional direction

In addition, the trajectory of the sun gear center can reflect the effect of the spalling on the sun gear. In time duration [31*T-31*5*T], the trajectory of the sun gear center under two conditions (a spalling fault on the sun gear and a healthy planetary system) is shown in Figure 7. The figure indicates that the spalling defect on the sun gear will break the regularity of the trajectory of the sun gear center and result in more translational vibration of the sun gear than in the healthy case; this means a spalling defect on the sun gear has greater influence on the vibration level of the component in a translational direction.

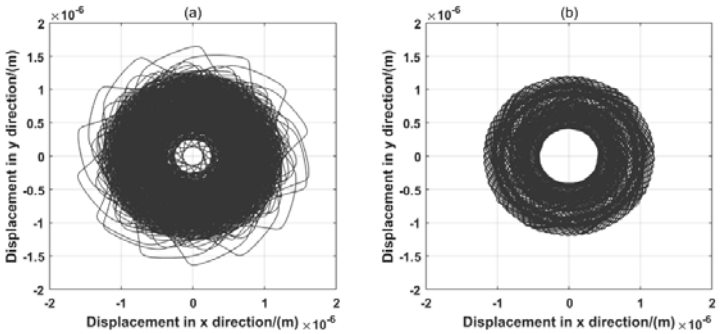

Figure 7. The trajectory of sun gear center: (a) spalling fault on the sun gear (b) healthy planetary system

As a consequence, in the case of a spalling fault localized on the sun gear, new frequency components appear at $nf_m + N\left[m\left(f_s - f_c\right)\right]$ (n, m are integers and n should obey the phase modulation law), where f_m represents mesh frequency, and f_s, f_c represent the rotational frequency of the sun gear and carrier respectively. The vibration amplitude will flatten out at higher levels. Its fluctuating amplitudes increase when a spalling defect appears.

If a spalling defect is seeded in the planet gear, every 21 meshing cycles (there are 21 teeth in a planet gear), the spalling tooth will mesh with the sun gear and ring gear one time. Figure 8 shows the acceleration of the sun gear in the torsional direction under two

conditions (healthy condition and planet gear with a spalling fault). The time duration of all signals in this figure is 4*21 meshing periods *T*, corresponding to four revolutions of the planet gear (the carrier is considered static). When we compare this to the healthy condition, it is obvious that there are four spikes in the signal, with the spalling fault on the planet gear meshing with the sun gear one time in one revolution of the planet gear. The fault symptom is obvious.

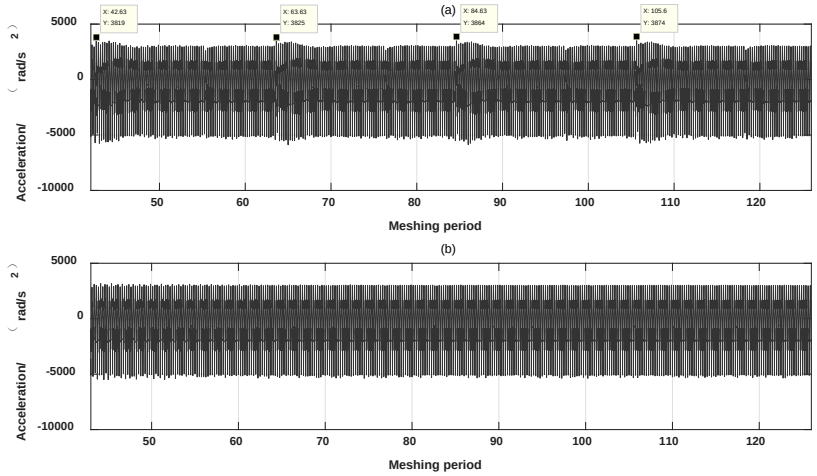

Figure 8. The dynamic response of the sun gear in torsional direction (a) spalling fault localized on planet gear (b) healthy planetary system

Figure 9 shows the frequency spectrum of the simulated acceleration signal corresponding to Figure 8. In the figure, sizable amplitudes show at the triple harmonics of mesh frequency under two conditions (healthy condition and a spalling fault on the planet gear). In the healthy condition, the gear mesh frequency and its harmonics dominate the frequency spectrum. When there is a spalling fault on the planet gear, a large number of sidebands appear around the gear mesh frequency and its harmonics. The frequency interval between sidebands is the characteristic frequency of the PGT with a spalling fault on the planet gear, or (f_p+f_c)= 20.72Hz, and the same phenomenon of amplitude modulation is observed: the amplitude of the mesh signal is modulated by the defect signal once per revolution of a planet gear relative to the carrier.

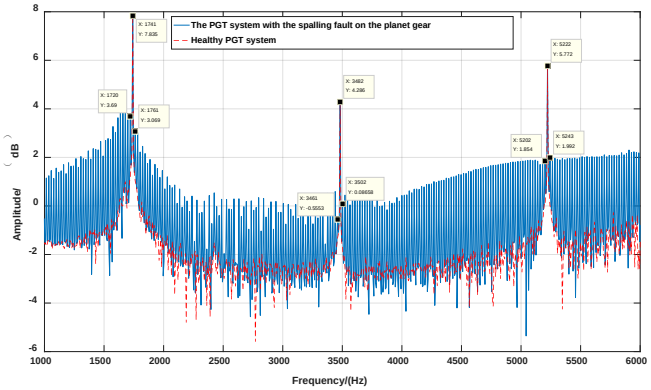

Figure 9. The frequency spectrum of the dynamic response of the sun gear in torsional direction

For the time period [21*T-21*5*T], the trajectory of the sun gear center under two conditions (a spalling fault localized on the planet gear and a healthy planetary system) is shown in Figure 10. The figure indicates that the spalling fault on the sun gear will break the regularity of the trajectory of the sun gear center and lead to a wider motion range than in the healthy condition.

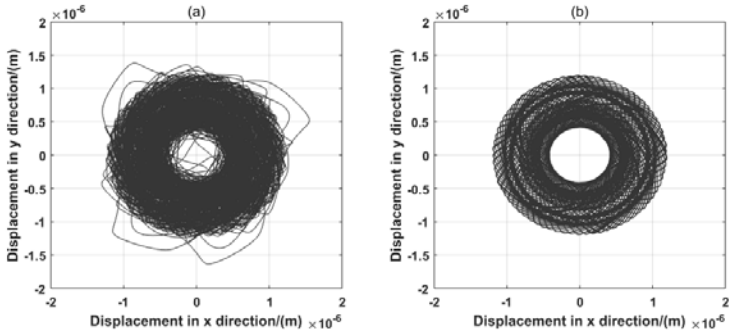

Figure 10. The trajectory of sun gear center: (a) spalling fault located on the sun gear (b) healthy planetary system

As a consequence, in the case of a spalling fault occurring on the planet gear, new frequency components appear at $nf_m + \left[m\left(f_p + f_c \right) \right]$ (n, m are integers and n should obey the phase modulation law), where f_p represents the rotational frequency of the planet gear. The vibration flattens with higher vibration levels in the torsional and translational directions.

In the case of a spalling defect localized on the ring gear, every 73 meshing cycles (there are 73 ring gears) the tooth on the ring gear with the spalling defect will mesh with the same planet gear. This means there could be a periodic impact impulse on the response of the planetary system. During this period, it also will engage with the other three planet gears one time. Figure 11 shows the torsional acceleration of the sun gear under two conditions (healthy and sun gear with spalling fault). The time duration of all signals given in this figure is 1*73 meshing periods, corresponding to one revolution of the ring gear (the carrier is considered static). When we compare this to the healthy condition, it is obvious that there are four spikes in the signal with the spalling fault on the sun gear. This corresponds to the spalling pair meshing with the planet four times in one revolution of the ring gear (there are four planets). The fault symptom is obvious.

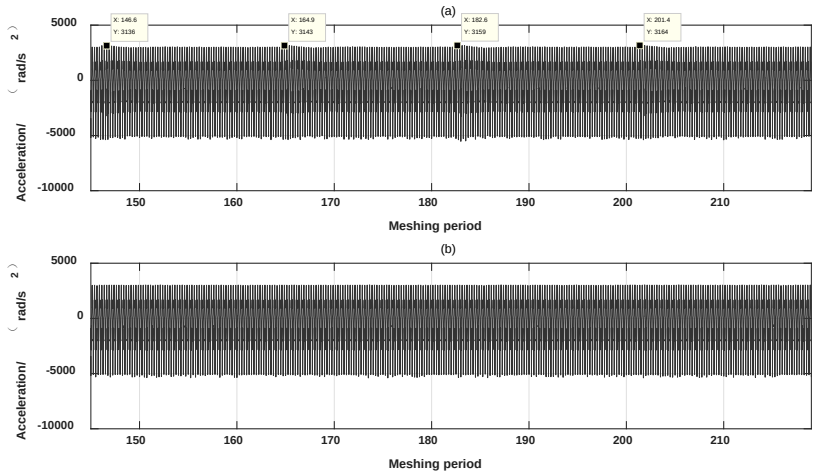

Figure 11: The dynamic response of the sun gear in torsional direction (a) spalling fault localized on the ring gear (b) healthy planetary system

Figure 12 shows the frequency spectrum of the simulated acceleration signal corresponding to Figure 11. As the figure shows, the presence of a spalling defect on the ring gear tooth can change the frequency spectrum structure, generating many sidebands around the fundamental mesh frequency and its harmonics. The frequency interval between sidebands is the characteristic frequency of the PGT with a spalling defect on the ring gear, or $N^*(f_c)$ = 23.85Hz. In this case, we observe an amplitude modulation of the mesh signal by the defect signal, once per revolution of a ring relative to the carrier.

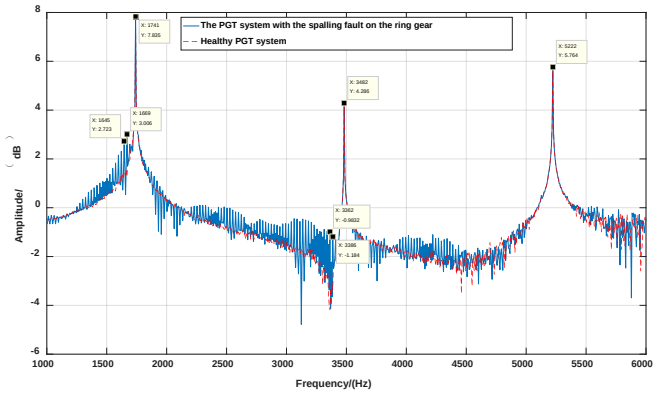

Figure 12. The frequency spectrum of the dynamic response of the sun gear in torsional direction

For the time period [2*73*T-3*73*T], the trajectory of sun gear center under two conditions (a spalling fault located on the ring gear and a healthy planetary system) is shown in Figure 13. The figure indicates that a spalling fault on the ring gear will lead to a slight disturbance in the trajectory of sun gear center compared to cases where the spalling fault is located on the sun gear or planet gear.

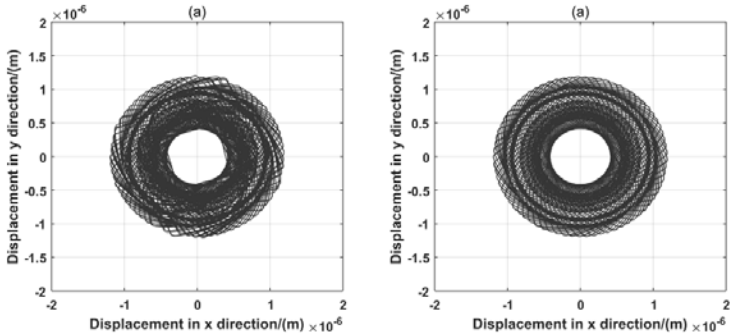

Figure 13: The trajectory of sun gear center: (a) spalling fault located on the ring gear (b) healthy planetary system

As a consequence, when a spalling defect occurs at the ring gear, the impulsive vibrations and sidebands can be observed in the dynamic response of the planetary gear set in time and frequency domains. New frequency components appear at $nf_m + Nmf_c$ (n, m are integers and n should obey the phase modulation law). The spectrum seems to be flattened at higher vibration levels, but compared to cases when a defect is localized on the sun gear or planet gear, this case (i.e., a spalling defect localized on the ring gear) has less influence on the dynamic response of the PGT system.

Conclusion:

The paper has provided an analytical formulation for mesh stiffness in the presence of a spalling defect. The mesh stiffness model, in which the spalling defect is seeded into the sun, planet, and ring gears in turn, is incorporated into a dynamic model of a PGT system to investigate the effect of tooth spalling defects. The dynamic responses computed in each of these cases show the dominance of the mesh frequency and its harmonics, with the presence of fault characteristic sidebands issued by the amplitude modulation caused by the spalling defect. The results can be applied to the condition monitoring and fault diagnosis of the planetary gear system.

Acknowledgement: This work is supported by the National Natural Science Foundation of China under Contract No.51475053 and Foundation of SKLMT-KFKT-201704 8: Diego Galar Lulea of technology wind farm condition monitoring.

References:

[1] M R Hoseini, M J Zuo. Literature review for creating and quantifying faults in planetary gearboxes. Reliability Research Lab, Mechanical Department, University of Alberta, May 2009.
[2] W Kim ,YL Ji ,J Chung. Dynamic analysis for a planetary gear with time-varying pressure angles and contact ratios. Journal of Sound & Vibration, 2012 , 331 (4) :883-901
[3] A Kahraman. Load sharing characteristics of planetary transmissions. Mechanism & Machine Theory, 1994 , 29 (8) :1151-1165
[4] A Kahraman. Planetary Gear Train Dynamics. Journal of Mechanical Design, 1994 , 116 (3) :713-720

[5] A.Kahraman, S.Vijayakar. Effect of Internal Gear Flexibility on the Quasi-Static Behavior of a Planetary Gear Set, Journal of Mechanical Design , 2001 , 123 (3) :408-415
[6] M Inalpolat, A Kahraman. A theoretical and experimental investigation of modulation sidebands of planetary gear sets. Journal of Sound & Vibration , 2009 , 323 (3) :677-696
[7] M Inalpolat, A Kahraman. A dynamic model to predict modulation sidebands of a planetary gear set having manufacturing errors. Journal of Sound & Vibration , 2010 , 329 (4) :371-393
[8] RG Parker, V Agashe, SM Vijayakar. Dynamic Response of a Planetary Gear System Using a Finite Element/Contact Mechanics Model. Journal of Mechanical Design, 2000 , 122 (3) :304
[9] T Sun, HY Hu. Nonlinear dynamics of a planetary gear system with multiple clearances. Mechanism & Machine Theory, 2003 , 38 (12) :1371-1390
[10] D.C.H. Yang, J.Y. Lin, Hertzian damping, tooth friction and bending elasticity in gear impact dynamics, J. Mech. Des. 109 (2) (1987) 189–196.
[11] X.H. Tian, Dynamic Simulation for System Response of Gearbox Including Localized Gear Faults. Master's thesis University of Alberta, 2004.
[12] Z. Chen, Y. Shao, Dynamic simulation of spur gearwith tooth root crack propagating along tooth width and crack depth, Eng. Fail. Anal. 18 (8) (2011) 2149–2164.
[13] RG Parker, J Lin. Mesh Phasing Relationships in Planetary and Epicyclic Gears. Journal of Mechanical Design , 2004 , 126 (2) :525-534
[14] RG Parker. A physical explanation for the effectiveness of planet phasing to suppress planetary gear vibration. Journal of Sound & Vibration , 2000 , 236 (4) :561-573